

Optical Properties of Anti-Reflective Coatings on P-N Silicon and their Response to Gamma-Irradiation



Abd El Wahab AA¹, Fayek SA¹, El Hossary FM², Hemada OM³, Mez T³, Hosni HM¹, Henaish AMA^{3,4*} and Abo El Kassem M²

¹Department of Solid State and Accelerator, National Center for Radiation Research and Technology (NCRRT), Egyptian Atomic Energy Authority (EAEA), Cairo, Egypt

²Department of Physics, Sohag University, Egypt

³Department of Physics, Tanta University, Egypt

⁴Nanotech Center, Ural Federal University, Russia

Submitted: March 05, 2022; Published: April 11, 2022

*Corresponding author: Henaish AMA, Department of Physics, Tanta University, Egypt, Nanotech Center, Ural Federal University, Russia

Abstract

The dc-pulsed plasma magnetron sputtering was used for depositing TiO₂, ZrO₂, and Ti₅₀-Zr₅₀ anti-reflection coating with thickness of 40 nm on p-n junction wafers and glass substrates. Furthermore, the antireflective properties of silicon nitride deposited elsewhere using plasma enhanced chemical vapor deposition (PECVD) were compared with those of metal oxide films. X-ray structural analysis reveals amorphous nature of the prepared films. The optical transmittance and reflectance measurements were investigated at room temperature in the wavelength range from 250 to 2500 nm. At long wavelengths, ZrO₂ has a slightly higher transparency than that of TiO₂ and Ti₅₀-Zr₅₀ oxide. On the other hand, the transparency at short wavelengths has different behavior. At about 300nm, a sharp decrease in the transparency of the three coatings was found. On the other hand, reflectance measurements show a decrease in reflectivity at 600 nm for ZrO₂ and Ti₅₀-Zr₅₀ oxide as compared to TiO₂. Samples irradiated with gamma rays at a dose of 5 kGray show different behavior in reflectivity due to displacement damage in Si-based cells.

Keywords: p-n Si cell; Dc-pulsed plasma magnetron sputtering; Anti-reflection coatings (ARC); TiO₂; ZrO₂; Ti₅₀-Zr₅₀ oxide

Abbreviations: PECVD: Plasma Enhanced Chemical Vapor Deposition; SCs: Solar Cells; ARC: Anti-Reflection Coatings

Introduction

Si-based solar cells (SCs) account for 90% of the current photovoltaic market. However, high production cost attitudes as an obstacle to their widespread performance [1]. Major industrial and researcher efforts are being made constantly to reduce the production cost while improving their power conversion efficiency. To do that, one of the main steps is to reduce reflection losses for solar cells, using anti-reflection coating (ARC) materials at the front surface of the cells, thereby coupling more sunlight into the cell to increase the photocurrent and efficiency [2].

Metal oxides nanostructure materials play an important role in the fields of optoelectronics and energy harvesting applications [3-5]. Oxides are a vital component of PV cells due to the various applications of oxides in PV cells. New oxide materials are being introduced for use in PV where numerous transition metal oxide

nanostructures with various morphologies have been synthesized using numerous techniques to achieve the requirements of the desired application [6-9]. Several highly transparent and high refractive index materials have been investigated as ARC in Si solar cells such as ZnS [10], CeO [11] TiO₂ [12] Ta₂O₅ [13], ZnO [14] and ZrO₂ [15] either in a single layer or multiple layer coating. Besides, the choice of SiNx nowadays as a highly transparent ARC material is attributed to the large band gap energy (5.1 eV) with little absorption between 300 and 1150 nm where Si solar cells operate [16]. ARCs with uniform thickness and good optical properties are synthesized by different vacuum-based processes such as physical vapor deposition, reactive sputtering and chemical vapor deposition including plasma-enhanced chemical vapor deposition PECVD and atomic layer deposition [17].

Thin-film TiO_2 has the potential to reduce the production cost of Si-based solar cells, depending on the cell design. This material can serve multiple purposes as anti-reflective coating (ARC) film, oxide passivation compatible film and doping source for emitter diffusion [18]. Zirconium as an abundant terrestrial metal (74 million metric) [19] is sufficient to produce Si solar cells on a terawatt scale [20]. Optical properties of ZrO_2 are considered as a suitable ARC on Si solar cells [21] where it has a large band gap of 6.1 eV [22] for cubic ZrO_2 and a refractive index value $n=2$ at 600 nm for dc-pulsed magnetron-sputtered ZrO_2 films which similar to PECVD SiN_x films [23]. Previously was also observed a similar trend in ZrO_2 films prepared by spray deposition [24] and by pulsed laser deposition [25] and by Magnetron sputtering [26-29]. In this work, the structural and optical properties of three ARC films, namely TiO_2 , ZrO_2 and $\text{Ti}_{50}\text{-Zr}_{50}$ oxide, were prepared by dc-pulsed magnetron sputtering to investigate the suitability of the prepared films for ARCs on p-n Si cells.

Experimental Procedure

Thin films preparation

Dc pulsed magnetron sputtering was used to coat a fixed thickness of 40nm thin films of TiO_2 , ZrO_2 and $\text{Ti}_{50}\text{-Zr}_{50}$ oxide on glass and Si (100) wafer p-n-junction. The films were grown by sputtering using ZrO_2 , TiO_2 and $\text{Ti}_{50}\text{-Zr}_{50}$ Oxide targets with purity of 99.99%, 50mm diameter and 3mm thickness. The glass substrates were ultrasonically cleaned with, methanol, acetone

and water. Si substrates were cleaned with diluted HF to remove native oxide from the surface. Sputtering is a type of physical vapor deposition technique that is widely used in both the laboratory and production. During sputtering an applied voltage is used to generate plasma that is confined close to a target material which ejects species that are then transferred to the substrate. Metal oxides can be grown directly from ceramic targets by sputter gas (argon), while metal targets can be sputtered using reactive oxygen together with the sputter gas. DC -pulsed magnetron sputtering can be used to deposit compact oxide coatings with relatively good properties at low temperatures. All details about magnetron sputtering can be found in separate reviews [30-32].

The schematic diagram of the dc-pulsed magnetron sputtering system is presented in Figure 1. Briefly, the system consists of a stainless-steel chamber with a diameter of 30 cm and was evacuated by turbo and rotary pumps to obtain a base pressure of 9×10^{-6} mbar. Argon gas (Ar) was introduced into the chamber to launch a total working gas pressure of 7×10^{-3} mbar which was measured by means of a manometer. The dc-pulsed power supply model: Pinnacle Plus pulsed was conducted to initiate the discharge. A powerful magnet was employed to ionize the target materials and direct it to settle on the substrate in the form of thin film. The selected substrates were fixed on a sample holder at a distance of 7cm from the target. The film thickness was adjusted to be around 40nm. The operating parameters of ZrO_2 , TiO_2 and $\text{Ti}_{50}\text{-Zr}_{50}$ oxide of the coatings are listed in Table 1.

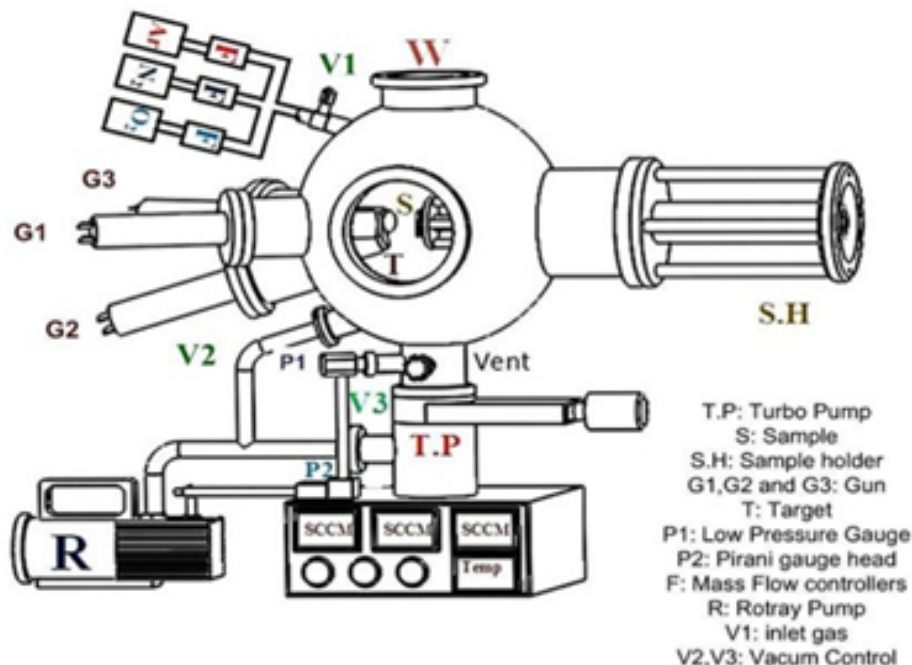


Figure 1: Schematic diagram of the dc-pulsed magnetron sputtering system [32].

Table 1: Operating parameters of various anti reflections coatings TiO_2 , ZrO_2 and $\text{Ti}_{50} - \text{Zr}_{50}$ oxide.

Target	TiO_2	ZrO_2	$\text{Ti}_{50} - \text{Zr}_{50}$
Base Pressure (mbar)	9×10^{-6}		
Work Pressure (mbar)	7×10^{-3}		
Gases	100%Ar	100%Ar	90%Ar + 10% O_2
Power (W)	150	400	120
Frequency (KHz)	150		
Reverse Time (μsec)	2		
Distance between target and substrate (cm)	7		
Film Thickness (nm)	40	40	40
Deposition Rate (nm/min)	3	0.5	1.6

Thin-film characterization

The optical properties of deposited thin films were investigated from transmittance and reflectance measurements at room temperature in the wavelength range of 200-1000nm using Jasco V-670 UV/VIS spectrophotometer. The structural of the deposited films were determined using Bruker D8 Advance diffract meter operated at low angle incidence using 40 keV and 40 mA with $\text{Cu-K}\alpha_1$ radiation ($\lambda = 1.54056 \text{ \AA}$).

Gamma rays irradiation effect

The output power of solar cells can be increased by improving the efficiency (η) and radiation resistance. In such a situation, radiation resistance is an important factor, because the continuous impact of high-energy particles damages the semiconductor lattice, degrades the performance of the cell, and thus limits its life. The MEGA gamma I irradiation facility in Egypt as type J-6500 was supplied by the Canadian Atomic Energy Corporation Ltd. at the National Center for Radiation Research and Technology in

Cairo, with a source of cobalt-60 used to irradiate samples with 5k grey [33,34].

Result and Discussion

XRD analysis

X-ray diffraction patterns of various antireflection coatings TiO_2 , ZrO_2 and $\text{Ti}_{50} - \text{Zr}_{50}$ oxide deposited on a glass substrate with a constant thickness $t=40 \text{ nm}$ demonstrated in Figure 2. It is obvious from the figure that the small diffraction peaks at 24° and 62° correspond to (1 0 1) and (2 0 0) diffraction planes for the anatase phase and another very small peak at around 45° corresponds to the (211) of the rutile phase for TiO_2 antireflection coating. The X-ray diffraction patterns of ZrO_2 displays very small diffraction peaks at 25.5° and 45.4° related to monoclinic structure oriented in (110) and (202) planes, respectively. The antireflection coating of $\text{Ti}_{50} - \text{Zr}_{50}$ oxide has a completely amorphous structure.

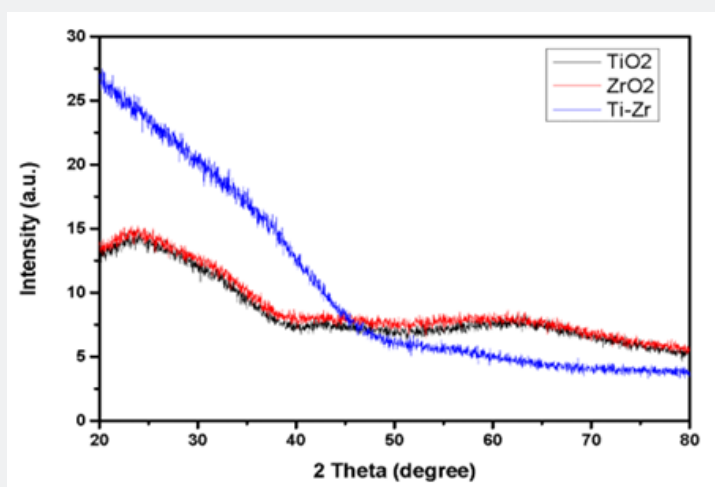


Figure 2: X-ray diffraction patterns of various antireflection coatings TiO_2 , ZrO_2 and $\text{Ti}_{50} - \text{Zr}_{50}$ oxide deposited on glass substrate with $t=40\text{nm}$.

Optical properties

The optical transmittance and reflectance of TiO₂, ZrO₂ and Ti₅₀-Zr₅₀ oxide on p-n silicon as a function of wavelength are shown in Figure 3. The appearance of interference fringes, which indicates that the films are homogeneous and flat, has been reported elsewhere [31]. The optical transmittance and reflectance depend on the type of ARCS and the category of deposition technique. In our case, the optical reflectance for

long wavelengths (>600nm) of different ARCs reduces close to zero. Moreover, the optical reflectance of ZrO₂ is the lowest with respect to that of anti-reflectors TiO₂ and Ti₅₀-Zr₅₀ oxide. At long wavelengths, ZrO₂ has slightly higher transmission compared to the others of anti-reflectors and p-n silicon. On the other hand, the transmission at short wavelengths has different behavior. At 300 nm it finds a decrease in transmission and starts to increase until the maximum transmission is at about 600 nm for Ty₅₀-Zr₅₀ oxide.

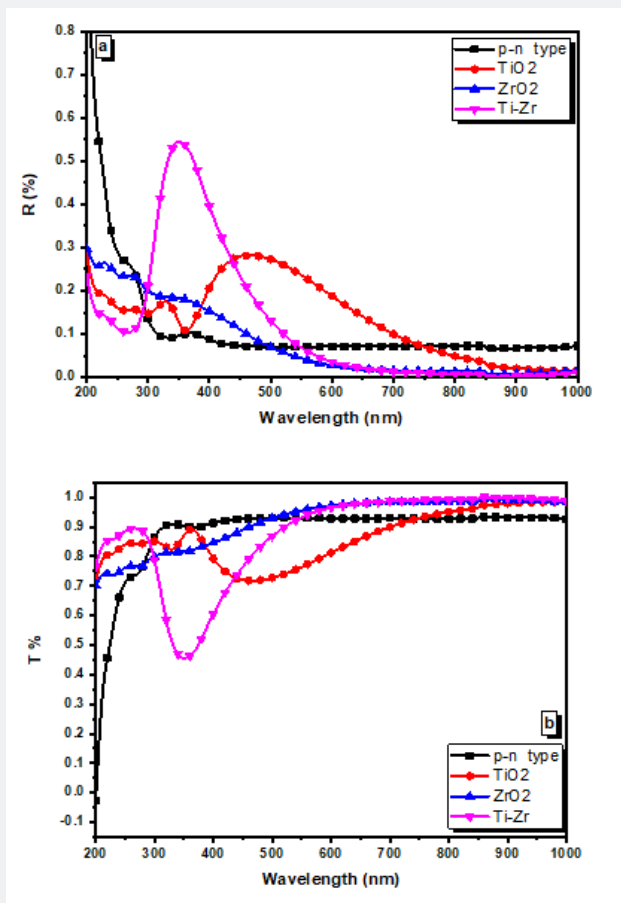


Figure 3: (a) Reflectivity and (b) Transmittance of various anti-reflection coating TiO₂, ZrO₂ and Ti₅₀-Zr₅₀ oxide on p-n junction at constant thickness t=40nm.

The optical absorption coefficient was calculated using the following equation:

$$\alpha = \frac{1}{d} \ln \frac{(1-R)^2}{T} \quad (1)$$

Where α is the optical absorbance and d is thickness of the film. The absorption coefficient α is related to the optical energy gap (E_g) and the frequency as given by Tauc equation:

$$(\alpha h\nu) = \beta (h\nu - E_g)^m \quad (2)$$

Where β is a constant that depends on the transition probability, h is the plank's constant, ν is the photon frequency,

E_g is the energy band gap. The optical energy gap is the minimum energy required to excite an electron from the valence band to the conduction band by an allowed optical transition. The value of the optical energy gap is usually determined by measuring the optical absorption coefficient as a function of the photon energy. The exponent (m) determines the type of direct and indirect transition that have values 1/2, 2, respectively.

Figure 4a illustrates the absorption coefficient depending on wavelength for the entire study spectra. This figure reflects the absorption edge in the visible region. It can be seen that at the

wavelength up to 1000 nm, all metal oxides precipitating at the pn junction have almost the same values of absorption coefficient except for $Ti_{50}-Zr_{50}$ oxide at 300 to 500 nm and TiO_2 at 400 to 650 nm. Figure 4b shows the variations of $(\alpha h\nu)^{0.5}$ versus the photon energy ($h\nu$) for the prepared samples. The values of the energy band gap (E_g) and refractive indices are listed in Table 2. The values of E_g are higher than those of SiN_3 at thickness of

75 nm. The increase in the energy band gap in the present work may be due to the up shift in the conduction band and downshift in the valence band leading to the band gap widening at 600nm. The results show that the band gap energy of $Ti_{50}-Zr_{50}$ oxide is the highest values than other antireflective coating TiO_2 and ZrO_2 . Moreover, the minimum energy gap value for ZrO_2 was obtained.

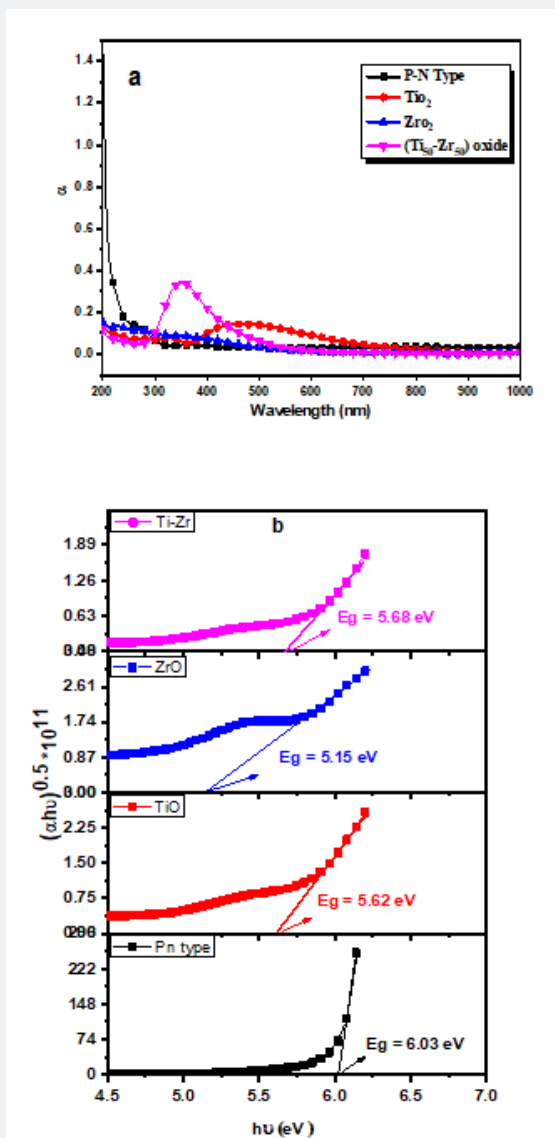


Figure 4: (a) Variation of absorption coefficient with wavelength (b) The dependence of $(\alpha h\nu)^{0.5}$ on photon energy ($h\nu$) for various ARCs TiO_2 , ZrO_2 and $Ti_{50}-Zr_{50}$ oxide.

Figure 5 compares the color of SiN_x thin film prepared by PECVD (75nm thickness), ZrO_2 film prepared by spray deposition with the same thickness, and ZrO_2 , TiO_2 and $Ti_{50}-Zr_{50}$ oxide prepared by dc-pulsed magnetron sputtering (40 nm thickness) on p-n junction substrates. The figure shows almost the same blue color for all samples, indicating that they have almost the

same refractive index. The refractive index of the ARC is one of the most important parameters for antireflection on Si solar cells. The optimum for a single-layer ARC can be calculated using the following equation (3):

$$n_{ARC} = \sqrt{n_{Si} \cdot n_{GI}} \quad (3)$$

Where n_{si} and n_{gl} are refractive index of silicon and glass, respectively. Glass has a typical refractive index of 1.4 and the refractive index of Si is 3.9 at 600 nm, so the optimum refractive index for the ARC is 2.34 [23]. This suggests that the refractive index of SiN_x , 2.0, is slightly below the optimum value and a high-index material is preferred for the ARC in Si solar cells. Antireflection

relies on quarter-wavelength destructive interference. For a film of a transparent material with a refractive index n and thickness d , the wavelength λ at which zero reflection occurs is calculated by equation (4):

$$d = \lambda / 4n \quad (4)$$

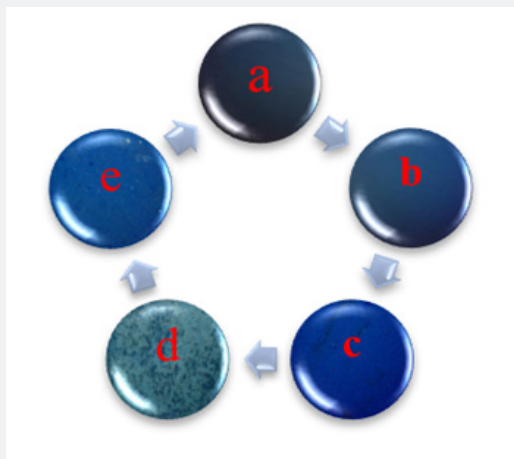


Figure 5: Optical microscope photo (5X) of (a) 75-nm SiN_x by PECVD, (b) 75-nm ZrO_2 by spray deposition, (c) 40-nm of ZrO_2 , (d) 40nm of TiO_2 and (e) photo 40 nm of $Ti_{50}-Zr_{50}$ oxide by dc-pulsed Magnetron Sputtering.

Where (λ) is the wavelength of the normal-incidence light in a vacuum. For solar cell applications, the refractive index and thickness of the ARC are designed to minimize the reflection at 600nm. This wavelength is close to the maximum power point of the solar spectrum.

The refractive index n as a function of λ can be calculated using the values k and R as follow:

$$n = \frac{1+R}{1-R} + \left[\frac{4R}{(1-R)^2} - k^2 \right]^{1/2} \quad (5)$$

k , extinction coefficient, measures the energy fraction dissipated of the incident beam of photons as a result of absorption and scattering of the original beam per unit length of the material. The variation of k for a material as a function of the wavelength is calculated from:

$$k = \frac{\lambda \alpha(\lambda)}{2\pi} ; \alpha(\lambda) = 2.303 \left(\frac{A}{d} \right) \quad (6)$$

Where (λ) is the coefficient of absorption, λ is the wavelength of the incident beam, A is the absorbance and d is the thickness (Figure 6).

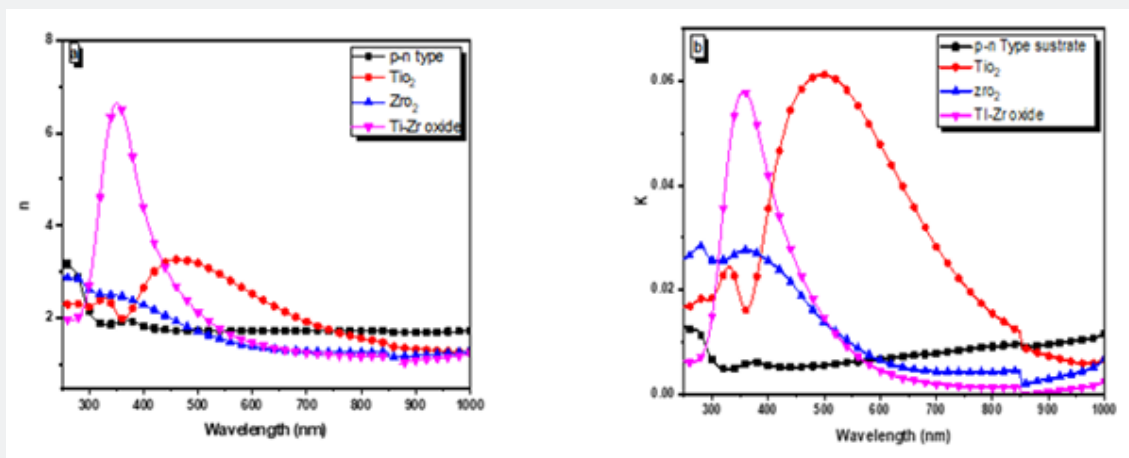


Figure 6: (a) The dependence of refractive index (n) and (b) the extinction coefficient (k) on wavelength for various (ARC) TiO_2 , ZrO_2 , $Ti_{50}-Zr_{50}$ oxide on the p-n junction.

It is observed that the k values increase with increasing wavelength up to 600 nm for TiO_2 and up to 350 nm for ZrO_2 and $\text{Ti}_{50}\text{-Zr}_{50}$ oxide and thus the k values are very sensitive to the antireflection coating (ARC) type in the visible region. However, at the longer wavelengths, all (ARC) TiO_2 , ZrO_2 and $\text{Ti}_{50}\text{-Zr}_{50}$ oxide are

close. In this work, it was found that TiO_2 has a refractive index of about 2.7 at $t = 40$ nm and ZrO_2 and $\text{Ti}_{50}\text{-Zr}_{50}$ oxide have a refractive index of about 1.95 and 2.19, respectively. Elsewhere, SiN_x has a refractive index of 2.05 at $t = 75$ with different deposition techniques as shown in Table 2 [15].

Table 2: The values of energy band gap E_g and refractive indices for various (ARC) TiO_2 , ZrO_2 , and $\text{Ti}_{50}\text{-Zr}_{50}$ oxide on p-n junction.

Type of ARCS	Energy band gap (ev)	Refractive index (N) at (600nm)
P-N type (substrate)	6.03	1.73
TiO_2 at $t=40\text{nm}$	5.62	2.7
ZrO_2 at $t=40\text{nm}$	5.15	1.95
$\text{Ti}_{50}\text{-Zr}_{50}$ oxide at $t=40\text{nm}$	5.68	2.19
Commercial SiN_x at $t=75$ nm	5.00	2.05

Effect of radiation on optical properties of (p-n) junction

In order to understand the behavior of samples with gamma-irradiation, one has to investigate the effect of gamma-radiation on solid material. Gamma-irradiation produces mainly ionization and excitation in the constituent atoms of the material. Moreover, it may also cause a small amount of atomic displacement depending

on its energy and the atomic number of the target atoms [33,35]. The effect of γ - radiation on optical properties of Si p-n junction cells coated with TiO_2 , ZrO_2 and $\text{Ti}_{50}\text{-Zr}_{50}$ oxide antireflection films with 40nm has been investigated at an irradiation dose of 5K Grey. The Optical reflectivity of the studied antireflection coatings before and after irradiation with dose 5K Grey is shown in Figure 7.

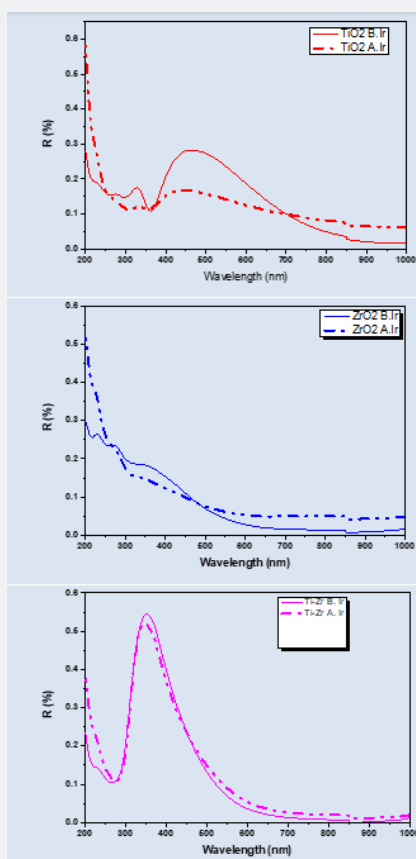


Figure 7: Reflectivity of various anti-reflection coating TiO_2 , ZrO_2 , $\text{Ti}_{50}\text{-Zr}_{50}$ oxide on p-n silicon junction before and after γ - irradiation with 5kGy.

It can be observed that there is a noticeable change in reflectivity of the samples after irradiation as compared with un-irradiated ones. For irradiated TiO_2 films, the decrease in reflectivity lies in the wavelength range from 400-700nm while the relative increase in its value from 700-1000 nm occurs for irradiated lies in the wavelength range from 300 to 700 films. For irradiated ZrO_2 , the decrease in reflectivity lies only in the wavelength range from 275-475 nm and for irradiated $\text{Ti}_{50}\text{-Zr}_{50}$ oxide has slightly difference with that of un-irradiated one. Based on the former notion, one has to discuss this effect on the evaporated films and the Si base as well. For anti-reflection coating films, γ -radiation may have a minor effect on their optical properties because of the following reasons

- a) The film thickness is ultra-thin and therefore radiation damage is minimal.
- b) The amorphous nature of the evaporating films may cause the radiation effect to be temporary with no permanent damage.

Therefore, the major effect of gamma-irradiation on samples reflectivity comes from its impact on the Si base. In other words, the change of reflectivity with irradiation may be attributed to active vacancies produced in the Si base by gamma radiation, where electrons are trapped at these vacancies. Figure 8 show

the variation of absorption coefficient with wavelength for various (ARC) TiO_2 , ZrO_2 and $\text{Ti}_{50}\text{-Zr}_{50}$ oxide on p-n silicon after gamma irradiation with 5KGrey. It can be observed that the intensity of the absorption decreases after irradiation by the ratio 2-4% at 600nm for TiO_2 . In addition, a noticeable change in the optical transitions between the bound states of the trapped electrons coupled with the vibration of the host Si crystal leads to vibrational absorption and emission as compared non-irradiated ones [34] and hence reduction in reflectivity over the certain optical range is expected to occur and vice versa. The values of energy band gap E_g increase after irradiation due to the increase of structural defects and the decrease at 600nm due to the damage of the substrate under the effect of gamma irradiation. The gamma irradiation induces changes in the refractive index over a wide range of wavelengths. The refractive index tends to be greater in the visible range (600nm) compared to the values measured in the other wavelengths. The induced refractive index increases after irradiation when moving toward the infrared range of the spectra. The gamma irradiation induces disordering of p-n junction, which can lead to broadening and spectral shift in the fundamental IR absorption band. The absorption modification results change in the refractive index of the materials. The values of energy band gap refractive indices before and after gamma irradiation with 5KGray are listed in Table 3.

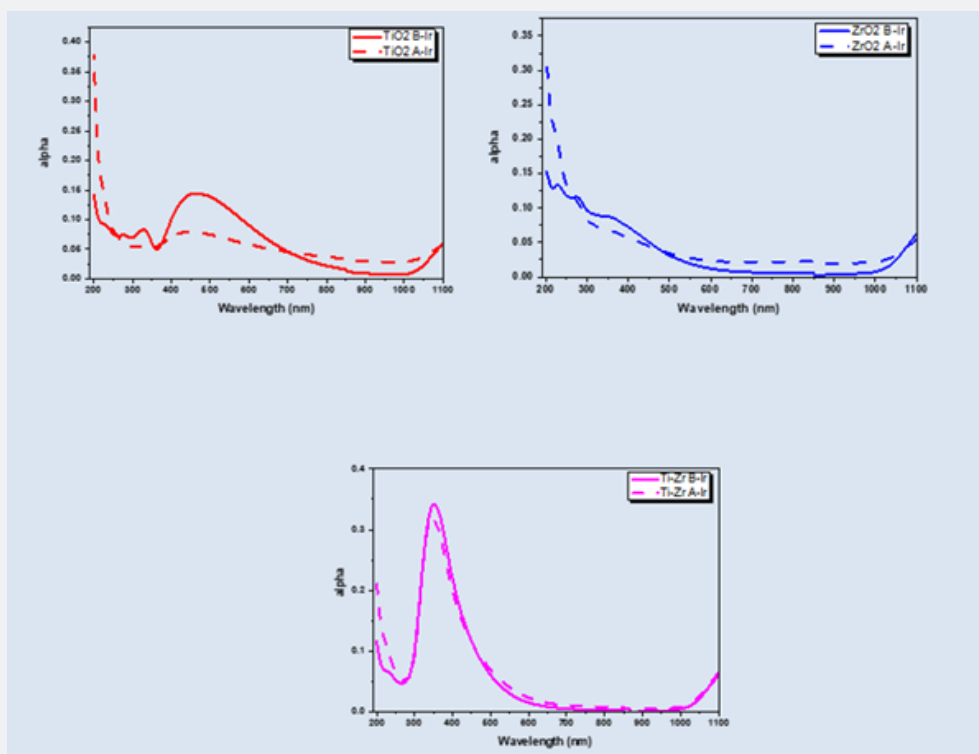


Figure 8: Variation of absorption coefficient with wavelength for various (ARC) TiO_2 , ZrO_2 , $\text{Ti}_{50}\text{-Zr}_{50}$ oxide on p-n junction before and after gamma - irradiation with dose 5kGy.

Table 3: The values of energy band gap (E_g) and refractive indices before and after gamma irradiation with 5kGy.

Type of ARCS	Energy band gap (ev) before irradiation	Energy band gap (ev) E_g after irradiation	Refractive index (n) before irradiation at (600nm)	Refractive index (n) after irradiation (600nm)
TiO ₂ at t=40nm	5.62	5.8	2.7	2.4
ZrO ₂ at t=40nm	5.15	5.43	1.95	1.8
Ti ₅₀ -Zr ₅₀ oxide at t=40nm	5.68	5.5	2.19	1.95
Commercial SiN _x at t=75nm	5	4.7	2.05	-

Conclusion

The possibility of using various metal oxides prepared by dc pulsed magnetron sputtering such as TiO₂, ZrO₂ and Ti₅₀-Zr₅₀ oxide as a coating for n-p Si junction has been studied. The structural and optical properties of dc magnetron sputtering TiO₂, ZrO₂ and Ti₅₀-Zr₅₀ oxide were studied and compared with commercial PECVD SiN_x. The X-ray diffraction patterns of the antireflection TiO₂, ZrO₂ and Ti₅₀-Zr₅₀ oxide show a completely amorphous structure. The optical reflectance for ZrO₂ and Ti₅₀-Zr₅₀ oxide drops to nearly zero in the range from 600 to 1000 and even lower than n-p Si junction alone. The decrease in reflectivity (10%) of the various coatings at 600 nm is similar to that of SiN_x. The results showed that the TiO₂, ZrO₂ and Ti₅₀-Zr₅₀ oxide has a refractive index of about 2.00 at 600 nm which is similar to that of SiN_x. The energy gap value and refractive indices of coated n-p Si increase slightly with that of uncoated substrate. Samples irradiated with gamma rays at a dose of 5 k Gray show different behavior in reflectivity due to displacement damage in Si-based cells. The results show that ZrO₂ thin films prepared by dc pulsed magnetron sputtering can be used as anti-reflective coatings for solar cells and other silicon-based photosensitive devices.

References

- (2018) Fraunhofer Institute for Solar Energy Systems, Photovoltaic Report.
- Diop MM, Diaw A, Mbengue N, Ba O, Diagne M, et al. (2018) Optimization and Modeling of Antireflective Layers for Silicon Solar Cells: In Search of Optimal Materials. *Mater Sci Appl* 9(8): 705-722.
- (2002) P Engineering, NS Wales, Novel Uses of Titanium Dioxide for Silicon Solar Cells, *Electr Eng*.
- Gangopadhyay U (2013) Efficiency Enhancement of Solar Cell by Introduction of Cerium Oxide along with Silicon Nitride. *Int J Renew Sustain Energy* 2(2): 46-50.
- Hocine D, Belkaid MS, Pasquinelli M, Escoubas L, Simon JJ, et al. (2013) Improved efficiency of multicrystalline silicon solar cells by TiO₂ antireflection coatings derived by APCVD process. *Mater Sci Semicond Process* 16(1): 113-117.
- Mohd Abdah MAA, Azman NHN, Kulandaivalu S, Sulaiman Y (2020) Review of the use of transition-metal-oxide and conducting polymer-based fibres for high-performance supercapacitors. *Mater Des* 186: 108199.
- Akbari A, Amini M, Tarassoli A, Eftekhari Sis B, Ghasemian N, et al. (2018) Transition metal oxide nanoparticles as efficient catalysts in oxidation reactions. *Nano-Structures and Nano-Objects* 14: 19-48.
- Sun XW, Kwok HS (1999) Optical properties of epitaxially grown zinc oxide films on sapphire by pulsed laser deposition. *J Appl Phys* 86(1): 408-411.
- Ghosh K, Gupta P, Pandey RK (2020) Optical properties tuning by sodium and magnesium co-doping in ZnO thin films for optoelectronic applications. *Mater Today Proc* 28: 177-181.
- Gangopadhyay U, Kim K, Mangalaraj D, Yi J (2004) Low-cost CBD ZnS antireflection coating on large area commercial mono-crystalline silicon solar cells. *Appl Surf Sci* 230(1): 364-370.
- Gangopadhyay U, Ray S, Panda E, Jana S, Das S (2013) Efficiency enhancement of solar cell by introduction of cerium oxide along with silicon nitride. *International Journal of Renewable and Sustainable Energy* 2(2): 46-50.
- Hocine D, Belkaid MS, Pasquinelli M, Escoubas L, Simon JJ, et al. (2013) Improved efficiency of multicrystalline silicon solar cells by TiO₂ antireflection coatings derived by APCVD process. *Materials Science in Semiconductor Processing* 16(1): 113-117.
- Rubio F, Denis J, Albella JM, Martinez DJM (1982) Sputtered Ta₂O₅ antireflection coatings for silicon solar cells. *Thin Solid Films* 90(4): 405-408.
- Aurang P, Demircioglu O, Es F, Turan R, Unalan HE (2013) ZnO nanorods as antireflective coatings for industrialscale single crystalline silicon solar cells. *Journal of the American Ceramic Society* 96(4): 1253-1257.
- Shin WJ, Huang WH, Tao M (2019) Low-cost spray-deposited ZrO₂ for antireflection in Si solar cells. *Mater Chem Phys* 230: 37-43.
- Verlaan V, Verkerk AD, Arnoldbik WM, Bakker R, Houweling ZS, et al. (2009) The effect of composition on the bond structure and refractive index of silicon nitride deposited by HWCVD and PECVD. *Thin Solid Films* 517(12): 3499-3502.
- Krogman KC, Druffel T, Sunkara MK (2005) Anti-reflective optical coatings incorporating nanoparticles. *Nanotechnology* 16(7): S338-343.
- Witit-anun N, Kasemanankul P, Chaiyakun S, Limsuwan P (2009) Structures and optical properties of TiO₂ thin films deposited on unheated substrate by DC reactive magnetron sputtering. *Kasetsart. J Nat Sci* 43(5): 340-346.
- French RH, Glass SJ, Ohuchi FS, Xu YN, Ching WY (1994) Experimental and theoretical determination of the electronic structure and optical properties of three phases of ZrO₂. *Phys Rev B* 49(8): 5133-5142.
- Tao M (2014) *Terawatt Solar Photovoltaics – Roadblocks and Opportunities*. London: Springer.
- Winchell AN, Winchell H (1964) The microscopical characters of artificial inorganic solid substances: Optical properties of artificial minerals pp. 439.
- Cho HJ, Hwangbo CK (1996) Optical inhomogeneity and microstructure of ZrO₂ thin films prepared by ion-assisted deposition. *Appl Opt* 35(28): 5545-5552.

23. Martin N, Rousselot C, Rondot D, Palmino F, Mercier R (1997) Microstructure modification of amorphous titanium oxide thin films during annealing treatment. *Thin Solid Films* 300(1-2): 113-121.
24. Shin WJ, Wang L, Tao M (2017) Low-cost spray deposited ZrO_2 for passivation and antireflection on p-type Si. *IEEE 44th Photovolt. Spec Conf PVSC* pp. 3435-3438.
25. Balakrishnan G, Thanigaiarul K, Sudhakara P, Song JI (2013) Microstructural and optical properties of nanocrystalline undoped zirconia thin films prepared by pulsed laser deposition. *Appl Phys A Mater Sci Process* 110: 427-432.
26. Suhail MH, Moha RG, Mohan S (1992) DC reactive magnetron sputtering of titanium structural and optical characterization of TiO_2 films. *J Appl Phys* 71(3).
27. Sahu BB, Jin SB, Xiang PJ, Kim JB, Han JG (2018) Effect of inductively coupled plasma and plasma parameters on magnetron sputtered Al-Doped ZnO highly conductive thin films at low-temperature. *J Appl Phys* 123(20).
28. Sahu BB, Lee MW, Long W, Han JG (2020) Role of plasma parameters on the characteristic's properties of flexible transparent ITO films deposited by 3D facing and planar facing magnetron sources. *AIP Adv* 10(10).
29. Misra P, Ganeshan V, Agrawal N (2017) Low temperature deposition of highly transparent and conducting Al-doped ZnO films by RF magnetron sputtering. *J Alloys Compd* 725: 60-68.
30. (2018) US Geological Survey, Mineral Commodity Summary.
31. Pearton SJ, Norton DP, Heo YW, Steiner T (2005) Recent progress in processing and properties of ZnO. *Prog Mater Sci* 50(3): 293-340.
32. El Hossary FM, El Rahman AMA, Raaif M, Qu S, Zhao J, et al. (2018) Effect of DC-pulsed magnetron sputtering power on structural, tribological and biocompatibility of Ti-Zr-N thin film. *Appl Phys A Mater Sci Process* 124(1): 1-12.
33. Hughes AE, Polley D (1975) *Real Solids and Radiation*. Wykeham Publications, London, UK.
34. Fox M (2001) *Optical properties of solids*. Oxford University Press Inc. New York, UK.
35. Billington DS, Crawford JH (1961) *Radiation Damage in Solids*. Princeton University Press, Princeton, NJ.



This work is licensed under Creative Commons Attribution 4.0 License
DOI: [10.19080/JOJMS.2022.07.555702](https://doi.org/10.19080/JOJMS.2022.07.555702)

**Your next submission with JuniperPublishers
will reach you the below assets**

- Quality Editorial service
- Swift Peer Review
- Reprints availability
- E-prints Service
- Manuscript Podcast for convenient understanding
- Global attainment for your research
- Manuscript accessibility in different formats
(Pdf, E-pub, Full Text, Audio)
- Unceasing customer service

Track the below URL for one-step submission

<https://juniperpublishers.com/submit-manuscript.php>